AGU ADVANCING EARTH AND SPACE SCIENCE

Space Weather®

RESEARCH ARTICLE
10.1029/2021SW002766

Geomagnetic Storm Occurrence and Their Relation With Solar Cycle Phases

Paula I. Reyes[1], Victor A. Pinto[2], and Pablo S. Moya[1]

[1]Departamento de Física, Facultad de Ciencias, Universidad de Chile, Santiago, Chile, [2]University of New Hampshire Durham, Institute for the Study of Earth, Oceans, and Space, Durham, NH, USA

Key Points:

- Geomagnetic storms are characterized by solar cycle (SC) and phases using a log-normal distribution fitted using maximum likelihood method
- SC24 behaved similarly to the minimum phase of the past five SCs in terms of the intensity of the storms that occurred
- Descending phase characteristic lognormal coefficient correlates with the following maximum phase and may predict strength of SC25

Supporting Information:

Supporting Information may be found in the online version of this article.

Correspondence to:

P. S. Moya,
pablo.moya@uchile.cl

Citation:

Reyes, P. I., Pinto, V. A., & Moya, P. S. (2021). Geomagnetic storm occurrence and their relation with solar cycle phases. *Space Weather*, *19*, e2021SW002766. https://doi.org/10.1029/2021SW002766

Received 19 MAR 2021
Accepted 9 AUG 2021

Abstract

Using a time series of geomagnetic storm events between 1957 and 2019, obtained by selecting storms where D_{st} <−50 nT, we have analyzed the probability of occurrence of moderate, intense, and severe events. Considering that geomagnetic storms can be modeled as stochastic processes with a log-normal probability distribution over their minimum D_{st} index, the dataset was separated according to solar cycle (SC) and SC phases, and the distributions of events were fitted through maximum likelihood method in order to characterize the occurrence of storms in each cycle and phase, and then compare those occurrences to the SC24. Our results show that there is a strong dependence between the occurrence of intense storms, with D_{st} < −100 nT, and the strength of the SC measured by the sunspot numbers. In particular, SC24 is very similar to SC20. However, when comparing the occurrence of storms by SC phases, events tend to show similar activity toward the minimum phase and have significant differences in the maximum phases. By looking at the σ value—the fit log-normal distribution "width" parameter—characteristic of the occurrence rate of storms, we have found that the σ_{des} (the sigma value in the descending phase of one cycle) shows the highest correlation ($r = -0.76$) with σ_{max} (the sigma value in the maximum phase of *the next* cycle) which allows us to estimate the occurrence rate of storms for SC25 to be similar to those of SC21 and SC22, suggesting a more intense cycle than the one that just ended.

Plain Language Summary

Geomagnetic storms are a common occurrence on Earth, and they can have significant impact on our lives. The occurrence of geomagnetic storms depends on the strength of the 11 yr solar cycle (SC), and the different phases in it. Since we have been recording sunspot numbers (which roughly indicate the activity of the sun) for centuries, and the storm index D_{st} (a measurement of geomagnetic activity on Earth) for decades, we study in this manuscript the connection between the two dataset, this is, how sunspot number (and therefore SC) relates to the occurrence of geomagnetic storms. We found that the latest SC behaved in a way, that is, more characteristic of the phases of low activity (minimum phase) of the previous cycles. We also found that in general, the declining phase of a cycle tends to be connected to the maximum phase of the next cycle, which indicates that a prediction of the next cycle can be attempted. In that regard, our results suggest that the SC that just started should be stronger than the current cycle, but no the strongest of the past five cycles.

1. Introduction

Geomagnetic storms are global disturbances caused by the interaction between the Earth's magnetic field and magnetized plasma ejected from the Sun, when transfer of large amounts of energy to the magnetosphere occur. Although geomagnetic storm effects vary depending on the characteristics of each events, some common effects to most storms include a dayside compression of the magnetosphere (Borovsky & Denton, 2016; Cattell et al., 2017), enhancement of magnetospheric currents (Ganushkina et al., 2017; Stepanova et al., 2019), depletion and enhancement of trapped particles in the radiation belts (Moya et al., 2017; Turner et al., 2015, 2019), enhanced precipitation in the auroral regions (Engebretson et al., 2008; Longden et al., 2008), changes in the dynamics and properties of the ionosphere and geomagnetically induced currents on the Earth's surface (Pulkkinen et al., 2005; Shi et al., 2008), among others. Such broad and global response and the quick transfer of enormous amounts of energy to the Earth's magnetic field can also have significant impact in a wide range of technological instruments such as damages and disruptions to satellites and communication systems (Chapman et al., 2020; Wrenn, 2009; Wrenn et al., 2002), jamming of radio signals, global positioning system scintillation and disruptions, but can also pose a threat to human exploration at high latitudes and high altitudes through enhanced radiation doses. These events can result

(and have resulted) in technological disruptions, economic losses, and dangers to human life in the past and most likely in the future (Baker et al., 2004; Eastwood et al., 2017), thus, the study of geomagnetic storm occurrence and their intensity over time is fundamental to improve our forecasting models, and to prevent or mitigate the risk associated with them.

Storms are traditionally classified according to their impact in the magnetosphere by measuring the strength of the disturbances recorded in ground-based magnetometers at different latitudes around Earth and by processing them as a series of indices such as the Kyoto Disturbance storm time (D_{st}) index (World Data Center for Geomagnetism, Kyoto et al., 2015). D_{st} index is a measure of low-latitude, ground level perturbations measured at four magnetic observatories located at Hermanus, South Africa; Kakioka, Japan; Honolulu, Hawaii; and San Juan, Puerto Rico. It is a proxy to the strength and evolution of the magnetospheric ring current, and has been used to define a scale of severity of a particular geomagnetic storm (Gonzalez et al., 1994; Kamide & Chian, 2007). In general, the more negative the D_{st} index, the stronger the geomagnetic storm. When it comes to understanding the physical processes that determine the strength of a storm, we must look out at the Sun to determine their driver. Storms can be loosely classified in two big groups: coronal mass ejection (CME) driven storms and stream interaction region (SIR) storms, mostly associated with high-speed streams in co-rotational interaction regions (CIR). CME driven storms tend to be associated with explosive releases of energy from the sun while SIR are a product of persistent coronal holes developing in the Sun's surface. More importantly, their occurrence is closely related to the phase of the solar cycle (SC) with CMEs being more common during the maximum phase (Hayakawa et al., 2018; Riley & Love, 2017) and SIR occurring consistently during the descending phase (Tandberg-Hanssen & Emslie, 1988).

The relationship between solar activity and the SC has been known for a long time. The solar activity (and thus the phase of the SC), can be measured through sunspots: visual manifestations of the Sun's magnetic activity that increases as solar activity does, and can be divided in four phases (minimum, ascending, maximum, and descending), due to its near 11 yr periodic variation. The presence of sunspots on the Sun is related to CME, SIR, and solar flares. In addition, significant decreases in the D_{st} index are generally associated with storms produced by CMEs (Gosling et al., 1991; Kilpua et al., 2015), although solar flares and high-speed streams associated with coronal holes can also produce similar magnetospheric effects.

Several studies have explored and quantified the relation between storms and the SC (Kilpua et al., 2015; Zhuang et al., 2018), and have found that generally the magnitude and number of geomagnetic storms that occurred during a given SC increase as the number of sunspots increases, reaching its greatest value during descending phase, 2 or 3 yr after the maximum phase of each cycle (Le et al., 2013). In the case of severe events, their intensities are not related to the strength of the SC, but tend to occur near the maximum phase (Kilpua et al., 2015). In addition, as geomagnetic storms can be treated as stochastic processes, the probability distribution function (PDF) of geomagnetic storms occurrence as a function of the D_{st} index can be fitted with a log-normal distribution. This is believed to be due to different processes (SC dynamo action, the geo-effectiveness of the solar wind-magnetospheric coupling, and the dynamic evolution of a geomagnetic storm) all acting together (Love et al., 2015). Recently Reyes et al. (2019) showed that for very weak SCs (such as SC24) extrapolations based on log-normal statistics tend to overestimate geomagnetic storms occurrence rates even for small events. Thus, if the trend of weak SCs continue, using previous SCs data to forecast the next cycle would most likely be unreliable.

In order to understand the relationship between the occurrence of geomagnetic storms and the SC, and following Kilpua et al. (2015), Love et al. (2015), and Reyes et al. (2019) we perform a statistical study treating storms as stochastic processes with log-normal distribution function to characterize their occurrence rate as a function of their respective SC and SC phase. We then compare the results obtained from SC19 through SC23 with those obtained for SC24. Furthermore, by using the characteristic average and standard deviation (SD) values obtained for each distribution, we discuss the expected behavior of SC25.

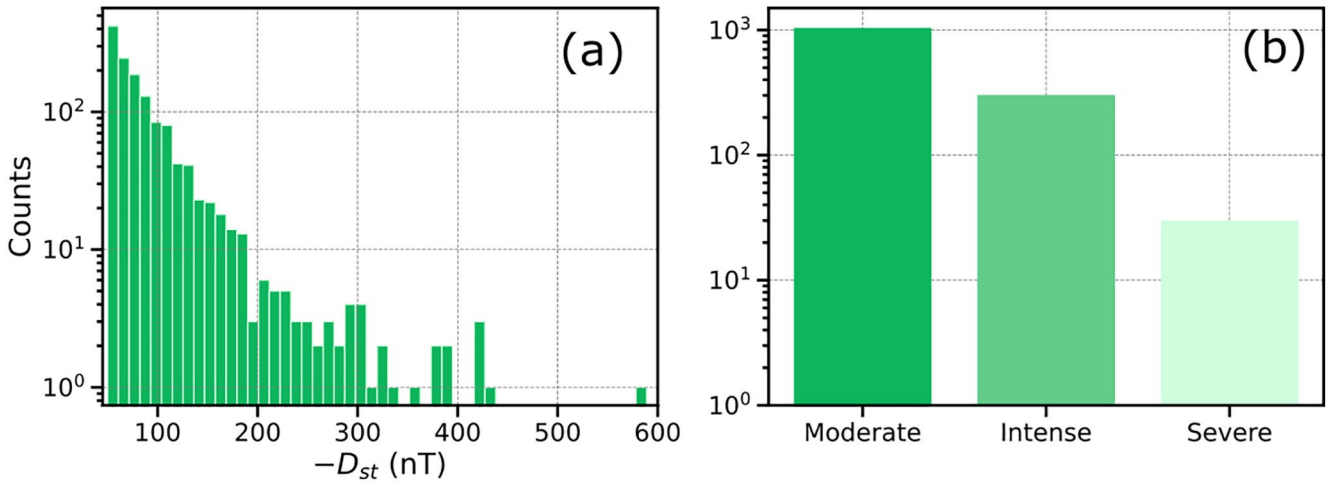

Figure 1. Distribution of geomagnetic storms between 1957 and 2019. (a) Histogram of D_{st} index minimum associated with each storm. (b) Distribution of geomagnetic storms according to their intensity.

2. Data and Methods

It is known that geomagnetic storms can be treated as stochastic processes (Pulkkinen et al., 2008), and the PDF of their occurrence can be fitted through a D_{st} index log normal distribution (Love et al., 2015; Reyes et al., 2019). In order to build the required PDF, here we consider two different indexes: D_{st} index to characterize the storm intensity, and sunspot numbers to identify solar activity and to separate the storm data on SCs and phases.

For our study, the D_{st} index data, with hourly resolution, was obtained from the World Data Center for Geomagnetism's at the University of Kyoto (World Data Center for Geomagnetism Kyoto et al., 2015), and is derived by averaging the deviation of the horizontal component of the ground magnetic field using four different observatories located in Kakioka, Honolulu, San Juan, and Hermanus. This historical index is available from 1957 to 2019, and therefore covers five complete SCs (SC20–SC24) plus more than 50% of SC19. The dataset is composed by ∼543,120 hourly D_{st} values. We use the D_{st} index to determine geomagnetic storm occurrence by locating its minimum value reached during the main phase, given that is, less than −50 nT. A storm is considered as an independent event if its separated for at least 2 days between consecutive D_{st} minima. Thus, from 1957 to 2019, we identified 1,369 geomagnetic storms, with values between $-589\ \text{nT} \leq D_{st} \leq -50\ \text{nT}$ (The complete list of 1,369 storms can be found in the Supporting Information S1). Figure 1a shows the storm distribution according to D_{st} index minimum and Figure 1b shows events grouped according to the storm intensity defined following typically used ranges on the D_{st} minimum value (see e.g., Gonzalez et al., 1994 and references therein). Namely, moderate ($-100\ \text{nT} < D_{st\,min} \leq -50$ nT), intense ($-250\ \text{nT} < D_{st\,min} \leq -100$ nT), and severe storms ($D_{st\,min} \leq -250$ nT). From Figure 1, we can observe that during the past five SCs there is a relatively sharp cutoff for $D_{st\,min} < 450$ nT. The only case outside this threshold is the March 1989 geomagnetic storm event ($D_{st\,min} = -589$ nT), that can be considered as an outlier, although an outlier that will not be excluded from our analysis.

The dataset of sunspots number (SSN) was obtained from World Data Center for the Production, Preservation and Dissemination of the International Sunspot Number (SILSO World Data Center, 1957–2019), with hourly time resolution. To determine the SCs thresholds, we calculated the smoothed sunspot index as follows: taking a yearly moving average with 1 week resolution, and then defining a cycle as the period of time between two consecutive minimum values. To separate the phases we use the same criteria as in Hynönen (2013) and Kilpua et al. (2015). To define the ascending phase, we first calculate the mean smoothed SSN number between the minimum phase and the subsequent maximum phase, then the ascending phase corresponds to the time period in which the SSN values lie between the mean SSN value ±1 SD from the mean. In the same fashion, the descending or declining phase is defined by calculating the mean smoothed SSN number in between the maximum phase and the subsequent minimum phase and then estimating the

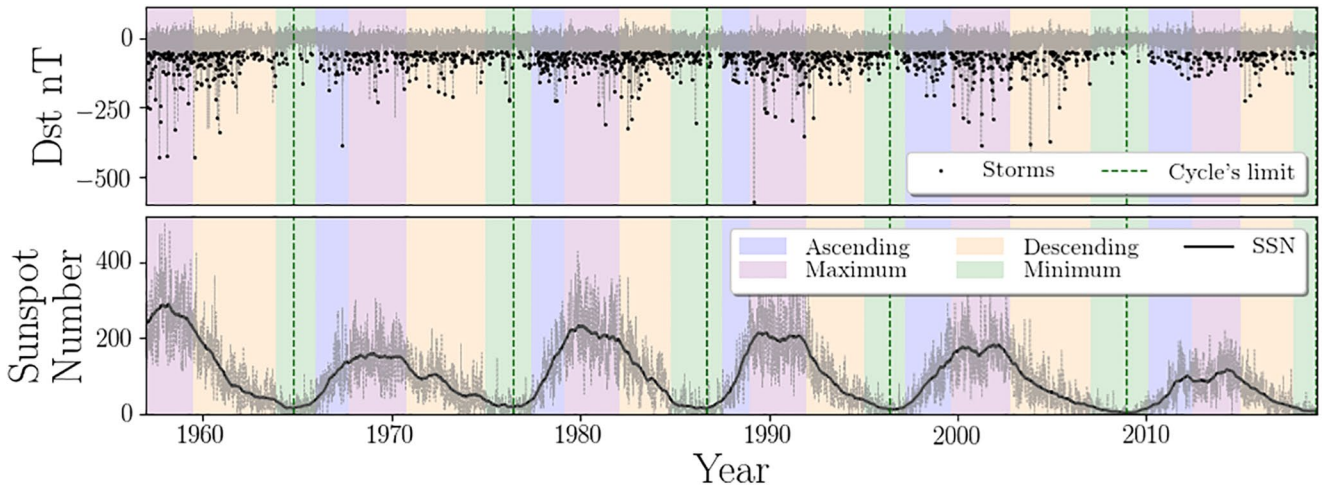

Figure 2. (Top) A total of 1,369 storms found with $D_{st} < -50$ nT between 1957 and 2019. (Bottom) Raw SSN count are shown in gray with black lines to indicate yearly moving average sunspot number. Colored blocks identify each phase, and vertical dashed lines mark SC limits.

time period in which the values lie between the smoothed mean ±1 SD. Following these definitions, the maximum and minimum phases are the time periods between ascending and descending phases of a given cycle, or descending and ascending phases of two consecutive cycles (a table with the dates for the start and end of each cycle and their phases can be found in the Supporting Information S1). Figure 2 shows a time series of geomagnetic storms and sunspot numbers separated by SC (vertical lines) and their respective phases. Top panel shows the D_{st} index (gray), with black dots indicating the geomagnetic storms. The bottom panel shows the raw data for sunspot numbers (gray), with a black line representing the smoothed sunspot index.

3. Analysis and Results

From Figures 1 and 2 is relatively clear that storms occur over a wide range of different magnitudes with great variability from SC to SC. Figure 3 explores that variability by grouping storms according to their SC and intensity. Figure 3a, shows geomagnetic storm occurrence histograms grouped by SC. It can be seen that the decrease in counts as $D_{st\,min}$ decreases (figure shows $-D_{st\,min}$) is different from cycle to cycle, with SC20 presenting the sharpest decrease, and SC19 and SC23 presenting the slowest decrease in occurrence.

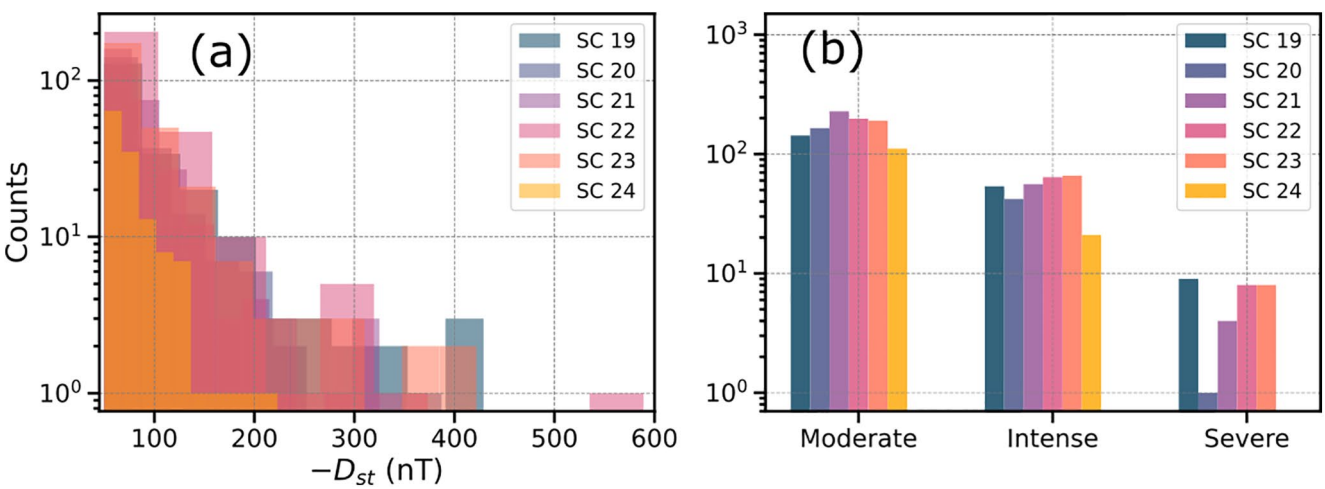

Figure 3. Distribution of geomagnetic storms between 1957 and 2019 separated by SC and storm intensity. (a) Histogram of D_{st} index minimum associated with each storm for each SC. (b) Distribution of geomagnetic storms according to their intensity for each cycle.

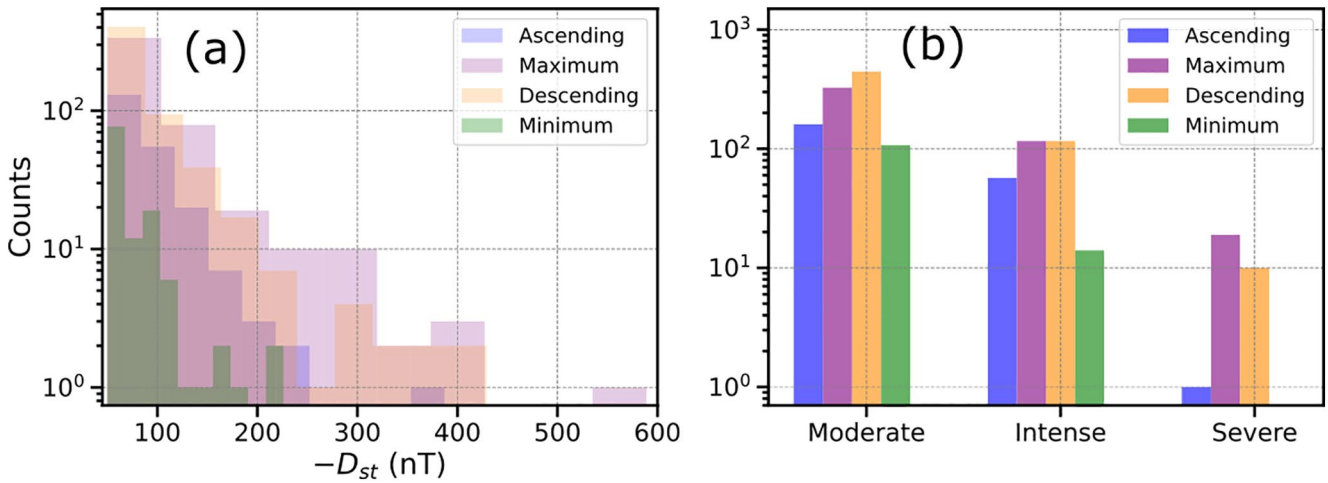

Figure 4. Distribution of geomagnetic storms between 1957 and 2019 separated by solar cycle (SC) phase and intensity. (a) Histograms of D_{st} index minimum for different SC phases. (b) Distribution of geomagnetic storms according to their intensity for each phase.

Figure 3b presents the storm occurrence grouped by category for the different SCs, in logarithmic scale. Here, SCs: SC21, SC22, and SC23 (more active in terms of SSN) were more active in geomagnetic activity in all storm categories, this is they present a higher count of events. On the contrary, the less active SCs: SC20 and SC24 in terms of SSN, consistently exhibit less geomagnetic storm activity (storm count) in all categories. It is important to mention that while SC19 shows a significantly smaller number of moderate storm events, the first minimum and ascending phases are not covered by the dataset which most likely explain the anomaly.

Additionally, storm occurrence is strongly affected by the phase of the SC (Kilpua et al., 2015). Figure 4 shows the occurrence rate of geomagnetic storms grouped according to the phase in which they occurred regardless of cycle. Figure 4a shows that in terms of $D_{st,min}$ storms occurring during the minimum phases occur less often and are less likely to be of large intensity. On the other hand, during the maximum phases we see the highest concentration of storms of $D_{st,min} < 200$ nT. In terms of the number of storms in each of our categories, Figure 4b shows that for moderate and even intense storms the occurrence is dominated by the descending cycle. This can be explained by the fact that storms associated to coronal holes are most common during the descending phase, but also due to the fact that descending phases tend to last longer than all the other phases (phase duration can be found in the Supporting Information S1). Storms during the maximum phase do catch up in number with the descending phase for moderate and intense events, and are dominant for severe events.

3.1. Log-Normal Representation of Geomagnetic Storms

Given that storm occurrence and their intensity can be fitted as a log-normal distribution (Love et al., 2015; Reyes et al., 2019), we want to obtain the characteristic coefficients of the distributions for all storms, and for storms separated by the SCs and phases. Following Figures 3 and 4, we expect the procedure to give valuable information to be used to estimate ranges of occurrences of different events for future SCs. As shown in Love et al. (2015), the occurrence probability F for an event with size exceeding $x = -D_{st}$, considering a log-normal process can be calculated as

$$F(x \mid \mu,\sigma^2) = \frac{1}{2}\mathrm{erfc}\left[\frac{\ln(x) - \mu}{\sqrt{2\sigma^2}}\right], \quad (1)$$

where μ and σ represent the average and SD of the distribution, respectively, and erfc is the complementary error function. The $-D_{st,min}$ distribution will be fitted through the following methods: maximum likelihood (ML) and least squares (LS) fits (assuming that data correspond to a log-normal function as Equation 1), and also a linear fit using a power law expression (powerlaw fit). Furthermore, we want to use the fits to extrapolate the occurrence of storms, and we calculate the associated errors using the bootstrap method, a

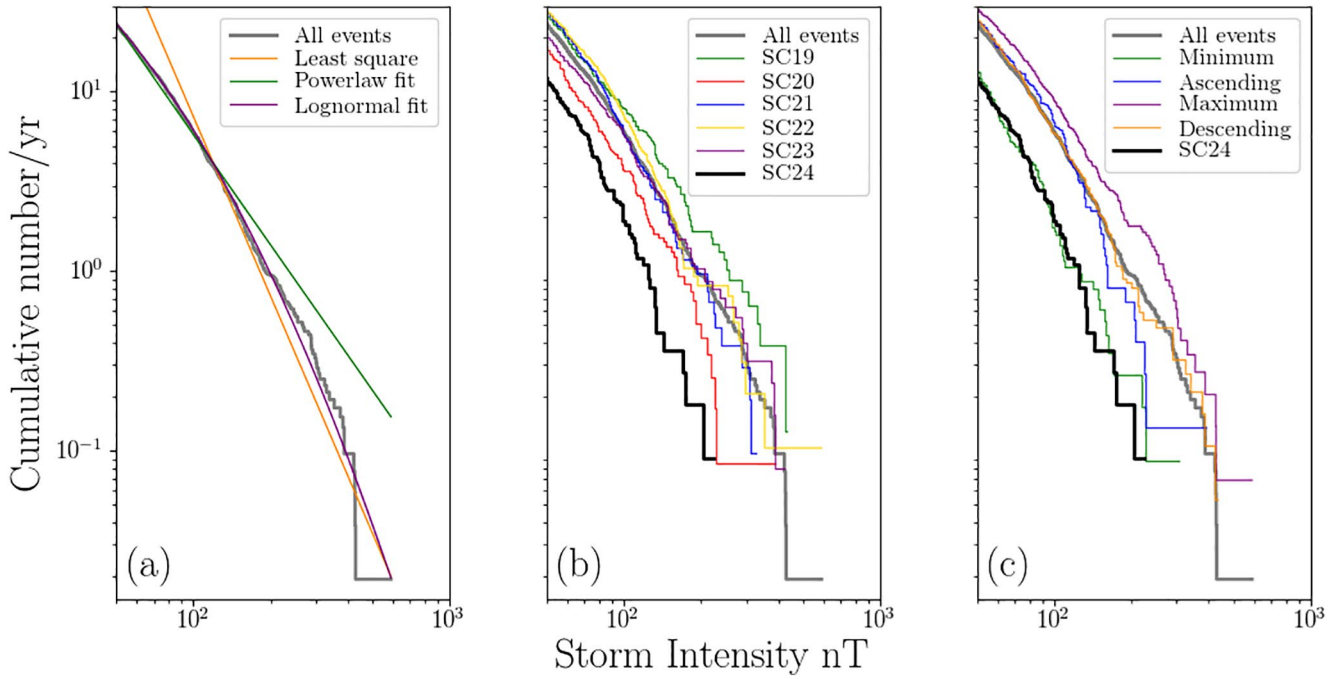

Figure 5. (a) Three different fits to cumulative number of storms per year (cumulative exceedances) for all events. (b) Cumulative exceedances separated by solar cycle (SC). (c) Cumulative exceedances separated by SC phase (results for SC24 are also included for comparison purposes.).

statistical technique to estimate the variation of point estimates, known as confidence intervals (CI; Kreiss & Lahiri, 2012). For this purpose, the $-D_{\mathrm{st,min}}$ data are re-sampled, and we calculate their median x^{*}_{median} to compute differences between the dataset median (x_{median}) and re-sampled median as $\delta^{*} = x^{*}_{\mathrm{median}} - x_{\mathrm{median}}$. Thus, our estimated 95% median bootstrap CI is given by $\delta_{95\%} = \left[x_{\mathrm{median}} - \delta^{*}_{.0025}, x_{\mathrm{median}} - \delta^{*}_{.0975}\right]$.

For our statistics, the data were grouped by SC and their respective phases, and the respective distributions of events were fitted using the three methods mentioned above (the complete list of μ and σ fits can be found in the Supporting Information S1). In order to compare each occurrence rate to the distributions obtained for SC24, we used a bootstrap method over the best fit to estimate the extrapolated storms median rate occurrence error with a 95% confidence. Figure 5 shows histograms of binned maxima storm value; that is, $-D_{\mathrm{stmin}}$. Figure 5a, shows the three different fits used over exceedances cumulative distribution functions (CDFs). A simple look lead us to conclude that ML fit (purple curve) gives the best representation of storms rate occurrence, as exhibits good agreement with the data for all type of storms (moderate, intense, and severe). On the contrary, the LS (orange line) and the powerlaw (green line) fits fail in reproducing the behavior of the CDFs for moderate or severe events, respectively. Thus, we will use the ML algorithm for the rest of our analysis.

Figures 5b and 5c, show the CDFs for the data separated by SC and SC phases, respectively. Analyzing by SC we observe that SC24 (black line) has the lowest storm rate occurrence, closely followed by SC20, consistent with the fact that they are the weakest cycles in terms of sunspot numbers and the least active cycles regarding storm occurrence as seen in Figure 3. This observation from the figure is backed by Table 1 that contains the estimated time between events (in years) for different ranges of $D_{\mathrm{st,min}}$. For example, SC24 and SC20 time between events for $D_{\mathrm{st,min}} \leq -50$ nT is 0.08 and 0.06 yr (29 and 22 days), respectively, while for the rest of the cycles is at most 0.05 yr (18 days). For stronger storms a similar trend is observed. SC24 and SC20 show significantly longer average waiting times between events than the rest of the cycles, and differences grow larger as storm size grows. Most notably, extreme events with $D_{\mathrm{st,min}} < -850$ nT (as estimated for the Carrington event; Siscoe et al., 2006) are expected to occur every 120 yr or every 44,000 yr if storm statistics follow the numbers obtained for SC23 or SC20, respectively.

Table 1
Bootstrap Results for Time Between Events (in Units of Years) and 95% Confidence Intervals for Maximum Exceedances for Each Solar Cycles (and Comparison With Time Between Events in SC24), and Each Minimum D_{st} Level

$-D_{st}$(nT)	SC19	SC20	SC21	SC22	SC23	SC24
50	0.04 [0.03, 0.05]	0.06 [0.05, 0.07]	0.04 [0.03, 0.05]	0.04 [0.03, 0.05]	0.05 [0.04, 0.06]	0.08
100	0.11 [0.09, 0.13]	0.25 [0.18, 0.29]	0.14 [0.11, 0.16]	0.12 [53.7, 75.2]	0.16 [0.13, 0.19]	0.52
200	0.62 [0.08, 0.82]	3.09 [3.17, 4.61]	2.19 [1.79, 3.26]	1.23 [0.84, 1.89]	1.12 [0.03, 1.51]	5.51
300	2.38 [0, 3.53]	24.7 [0, 42.1]	23.9 [0, 40.6]	10.5 [0, 17.6]	5.15 [0, 7.87]	-
400	7.3 [0, 11.7]	140 [0, 260]	190 [0, 341]	64.0 [0, 115]	18.0 [0, 30.8]	-
500	19.0 [0, 32.0]	660 $[0, 1.2\times10^3]$	110 $0, 2.2\times10^3$	310 [0, 580]	55.0 [0, 96.0]	-
600	45.0 [0, 79.0]	2.5×10^3 $0, 4.9\times10^3$	5.8×10^3 $0, 1.1\times10^4$	1.3×10^3 $0, 2.4\times10^3$	150 [0, 260]	-
850	270 [0, 500]	4.4×10^4 $0, 8.7\times10^4$	1.8×10^5 $0, 3.6\times10^5$	2.7×10^4 $0, 5.2\times10^4$	1.1×10^3 $0, 2.1\times10^3$	-

Figure 5c shows CDFs of events separated by SC phases. A remarkable observation is that SC24 behaves as the combination of all minimum phases of the previous cycles (green curve) in terms of rate occurrence, suggesting that SC24 reduced activity observed in sunspot number also impacted on storm occurrence rate. Table 2 seems to confirm this assumption since storms of −50, −100, and −200 nT occur every 0.08, 0.52, and 5.51 yr for SC24, respectively, all values within the 95% CIs of minimum phases rate occurrence and outside the CI of all other SC phases. From Figure 3 (right) and Table 2, we can also observe that the storm occurrence rate is clearly higher during maximum phase for all storms with $D_{st,min} < -100$ nT. Moreover, the results show that occurrence rates during ascending and descending phases are quite similar for moderate events ($D_{st,min} \geq -100$ nT), but the behavior of both phases differ for stronger storms, and the difference increases with increasing severity of the events. In particular, the bootstrap method predicts severe events with $D_{st,min} < -300$ nT to occur every 3, 10, 31, or 145 yr during maximum, descending, ascending, and minimum phase, respectively. Regarding extreme events, log-normal fits predict extreme events with $D_{st,min} < -500$ nT occurring every hundreds or thousands of years during descending, ascending and minimum phases. In comparison, the same algorithm predicts one of these events to occur every 34 yr approximately during maximum phase. Therefore, the $-D_{st,min} \sim 450$ nT cutoff observed in Figure 1 may indicate a minimum $D_{st,min}$ to consider for predictions of the next few SCs.

The numbers shown in Table 2 suggest that in order to make predictions about the strength of a cycle in terms of the occurrence of intense and especially severe events, the most reasonable time periods to look at are the maximum and descending phases, given that the occurrence rates contain CIs within the SC duration for events with $D_{st,min} > -400$ or $D_{st,min} > -300$ nT, during maximum and descending phases, respectively. Therefore, the possibility of having intense or severe events during the average

Table 2
Bootstrap Results for Time Between Events (in Units of Years) and 95% Confidence Intervals for Maximum Exceedances for Each Solar Cycle Phase (and Comparison With Time Between Events in SC24), and Each Minimum D_{st} Level

$-D_{st}$ (nT)	Minima	Ascending	Maxima	Descending	SC24
50	0.09 [0.08, 0.10]	0.04 [0.03, 0.05]	0.04 [0.03, 0.05]	0.04 [0.03, 0.05]	0.08
100	0.49 [0.20, 0.60]	0.15 [0.11, 0.17]	0.10 [0.09, 0.11]	0.15 [0.13, 0.16]	0.52
200	11.0 [0, 18.5]	2.45 [0, 3.75]	0.64 [0.26, 0.81]	1.45 [0.15, 1.98]	5.51
300	145 [0, 271]	30.7 [0, 53.8]	2.94 [0, 4.25]	9.61 [0, 14.9]	-
400	1.3×10^3 $0, 2.5\times10^3$	279 [0, 519]	10.8 [0, 16.9]	47.5 [0, 79.8]	-
500	8.6×10^3 $0, 1.7\times10^4$	1.9×10^3 $0, 3.8\times10^3$	33.6 [0, 55.6]	190 [0, 336]	-
600	4.6×10^4 $0, 9.0\times10^4$	1.1×10^4 $0, 2.0\times10^4$	92.0 [0, 160]	653 $0, 1.2\times10^3$	-
850	1.6×10^6 $0, 3.2\times10^6$	4.8×10^5 $0, 9.5\times10^5$	780 $0, 1.4\times10^3$	8.8×10^3 $0, 1.7\times10^4$	-

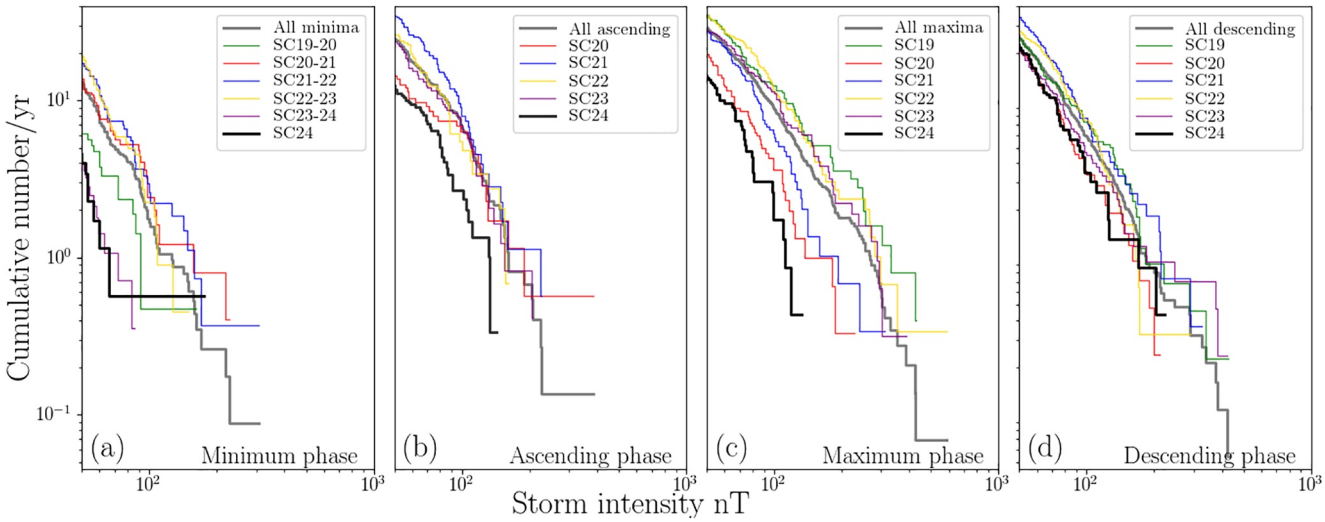

Figure 6. Cumulative exceedances for solar cycle (SC) phase separated by SC. From left to right each panel shows results for (a) Minimum, (b) Ascending, (c) Maximum, and (d) Descending phases, respectively.

duration of a SC should be determined by the activity during these phases and not the activity of a SC as a whole. To further explore this conjecture, we increase the scope of our analysis by fitting the phases of each SC separately, and comparing the results with the occurrence rates obtained previously. In our analysis, as minimum phases are shared between two subsequent SC, the notation used means that, for example, SC20–21 corresponds to the minimum phase between SCs: SC20 and SC21, and so on. It is important to note that the SC18–19 minimum phase was not considered here because there is no D_{st} record prior 1957. In addition, as our dataset ends in 2019 and the minimum phase SC24–25 is not over yet, for the current minima we only use data corresponding to SC24 and denote that minimum phase as SC24.

Figure 6a shows the occurrence rates of all six minimum phases considered in this study both individually and combined. We observe that SC20–21, SC21–22, and SC22–23 minima have the greatest occurrence rate of all minimum phases, and that coincides with the three most active cycles of the study in terms of SSN. On the other hand, SC19–20, SC23–24, and SC24 have the lowest rate occurrence, with ~ 5, 3, and 3 events per year with $D_{st,min} > -100$ nT, respectively. In terms of intensity, no storm D_{st} drops below −200 nT and therefore, the intensity of the storms is the lowest of all SC phases. SC19–20 and SC23–24 minimum phases, having a similar number of events per year, correspond to the start of the two less active cycles in our study. This suggest that the activity of a SC can be estimated by the behavior of its first years during the initial minimum phase, however, even if this is true (and here we make no attempt to prove it), this connection can be useful to make broad estimations about the occurrence of moderate events, but not necessarily the total strength of the cycle measured by the occurrence of intense or severe storms. Unfortunately, for SC25, the minimum phase is still ongoing, so considering the SC24–25 minimum phase to estimate the strength of SC25 is not possible.

For ascending phases, second panel of Figure 6b (SC19 ascending phase is not shown), indicates that SC21 has the higher occurrence rate for moderate storms, followed by SC22 and SC23 that behave similar to the average of all ascending phases. In comparison, SC20 and SC24 (the less active of all time series) exhibit much lower rates. In addition, as storm intensity grows, the number of events per year tend to be similar for all cycles, except for SC24 which its rate occurrence is always lower.

Further, if we observe maximum phases in Figure 6c, where all cycles reach their maximum smoothed sunspot number values, SC19, the most active of time series, have the largest rate occurrence for $D_{st,min} < -50$ nT, followed by SC22, being the third of most active cycles in SSN. For weaker cycles (i.e., SC24 and SC20 maximum phases), storm rate occurrence is the lowest, and storm severity is considerably weaker than during other maximum phases as the strongest storm during SC24 reached $D_{st,min} = -222$ nT, while

the 1989 event during SC22 had $D_{st,min} = -589$ nT. Thus, as expected, the storm occurrence data are in general ordered according to the SSN. Figure 6d shows all descending phases. This is possible the most complex panel. At first sight, there is not a clear difference between different cycles, suggesting that maybe most descending phases are essentially the same with ~11 – 12 storms per year for $D_{st} < -50$ nT, and as we go further through storms intensities, maximum values reaching between −200 and −500 nT). However, minor differences do exist, and although hard to visualize, the strongest cycles are not the same shown for the maximum phase. We are interested in further exploring those small differences to see if they show any correlation between them that could be useful for the prediction of the strength of a future SC. Previous studies have suggested that indeed a connection exists between different SCs, in particular, between the descending phase and the maximum phase of the following cycle (Dikpati et al., 2019; Feynman & Yue Gu, 1986; Leamon et al., 2020; McIntosh et al., 2019; McIntosh & Leamon, 2017). In the following section, and based on our characterization of the SCs, we explore that possible connection between phases.

3.2. Projections for SC25

We have fitted the geomagnetic storm occurrence as a log-normal distribution following Equation 1 and have calculated characteristic σ and μ parameters for each cycle and phase. The parameter σ, that corresponds to the SD of the function can be interpreted as the "width" of the distribution, and gives us a clue of how many large events are expected to occur. However, such comparison is correct only for distributions with similar μ values. In this case, considering all data and all μ values shown in Table S3, we can see that considering all cycles and phases the average value of μ is $\mu_{ave} = 4.11 \pm 0.22$ (a SD of just the 5.4%); namely, all obtained μ values are essentially the same and represent a most probable storm with $D_{st,min}$~−61 nT. Therefore, it is σ and not μ the value that will provide information about the differences between the distribution of events during different SCs and phases. Based on this and the assumption that some information of a SC carries through the next SC (i.e., that we can in fact, predict the next SC based on the current one) we have made comparison of the σ values of different phases, with phases of the next cycle. We have found that the only meaningful correlation occurs between σ_{des} and σ_{max} of the next SC. Figure 7 shows that correlation, and indicates where the prediction for SC maximum phase would be if we use a linear regression model to predict based on the characteristic σ_{des} of the SC24. In this case, given that $\sigma_{des,24} = 0.507$ we obtain that $\sigma_{max,25} = 0.561$.

The interpretation of this prediction must be treated carefully, especially if the result corresponds to a linear trend with so few data points. Nevertheless, to further quantify the statistical value of our prediction, we have have computed a p-value of 0.12, enough to make it better than random (especially for a calculation made with five points), but not good enough to be considered as a solid statistical result. However, and considering that the correlation coefficient is nonetheless elevated, we think that the discussion at least presents some merits. A $\sigma_{max,25} = 0.561$ suggest that the maximum phase of SC25 should be more active than SC20 and SC24, while at the same time being less active than SC21, SC22, and SC23. Comparing a distribution with $\mu = \mu_{max,24} = 4.228$ and $\sigma = \sigma_{max,24} = 0.301$ (as obtained for the maximum phase of SC24), and another with $\mu = \mu_{ave} = 4.11$ and $\sigma = \sigma_{max,25} = 0.561$ (as projected for SC25) will produce relevant differences not only for very large values of the $D_{st,min}$ index. For storms with a minimum D_{st} of −100, −200, or −300 nT, respectively, the CDFs of the distribution with the projected values for μ and σ will will be ~5, 715, or 71,593 times larger than the CDF of the distribution with $\mu_{max,24}$ and $\sigma_{max,24}$. In that regard, the large difference for extreme events with $D_{st,min}$ <−300 nT should be interpreted as a worst case scenario for the next cycle. However, as the differences are noticeable even for moderate and intense events (likely to occur even during the least active SC), a prediction or estimation of a significant larger value of , with , essentially constant, should not be considered as the most probable case, but at the same time does provide a projection for more than the extreme scenario.

Considering that there is a high correlation between storm rate occurrence and SSN, and that we utilize the SSN during the maximum phase to determine the strength of the cycle, our results suggest a SC25 that will be considerably stronger than SC24 with a maximum smoothed monthly sunspot number between 150 and 200, as opposed to some earlier predictions (see e.g., Bhowmik & Nandy, 2018; Shepherd et al., 2014; Svalgaard et al., 2005 and references therein) but in line with more recent studies (McIntosh

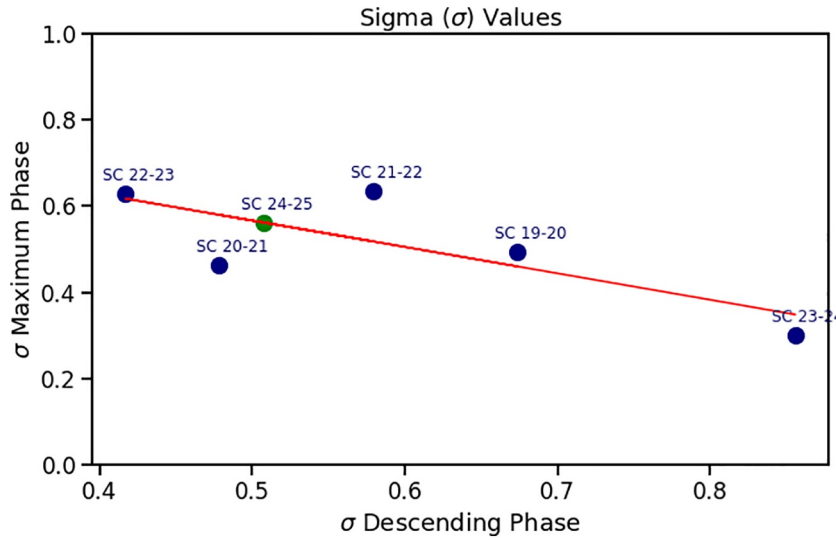

Figure 7. Linear fit between sigma of descending phase σ_{des} and sigma of maximum phase σ_{max} of the following SC.

et al., 2020). Naturally, several SCs will be needed before we can fully determine if this relation between descending phase and next maximum phase is real or not, so these results must be considered with a certain degree of skepticism. As the 2008–2010 solar minimum between SC23 and SC24 was unusually small, the trending shown in Figure 7 may change considerably if that data point is removed. Indeed, when we do so, statistical results change from a correlation coefficient of 0.77 (and a p-value of $p = 0.12$) when five SCs are considered, to a correlation coefficient of 0.28 (and $p = 0.72$) considering only four SCs without the SC23–24 minimum. Nevertheless, the projected value for sigma remains almost the same, changing from $\sigma_{max,25} = 0.561$ to $\sigma_{max,25} = 0.54$ when SC23–24 minimum is removed from the analysis. Therefore, even though the statistical significance of the result is much smaller, the prediction holds even for a four data points calculations, which emphasize the fact that more SCs are needed in order to corroborate or dismiss our method. However, previous studied have reported a strong correlation between the descending phase and the strength of the following SC in terms of the sunspot number (e.g., Dikpati et al., 2019; Leamon et al., 2020; McIntosh et al., 2019; McIntosh & Leamon, 2017), and also in terms of the relation between solar and geomagnetic activity, as shown by Feynman and Yue Gu (1986), using sunspot number and AA index time series.

4. Discussion and Conclusions

Considering geomagnetic storms occurred between 1957 and 2019, and time series of sunspot number during the same time span, we have analyzed the probability of occurrence of storm events and their relation with the SC. We have calculated rates of occurrence and statistics for geomagnetic storms during SCs SC19 through SC24, identifying the statistics of individual cycles and their phases. Our approach involved using a log-normal fit to the storm distributions using the ML method in order to establish a relationship between the characteristic parameters of the log-normal distributions (mean and SD) and the occurrence of geomagnetic activity during each cycle and each SC phase. Separating the events into moderate ($-50 > D_{st,min} > -100$ nT), intense ($-100 > D_{st,min} > -250$ nT) and severe ($-250 > D_{st,min}$ nT), we have found that the more active SCs (SC21, SC22, and SC23) in terms of SSN correspond to the cycle with higher occurrence of storms in all categories. Also, the SCs with the less number of sunspots (SC20 and SC24), as expected exhibit less geomagnetic storm activity.

Moreover, comparing the occurrence of storms by SC phases, event occurrence tends to be similar during minimum phases and have significant differences in the maximum phases. We separated the events according to SC phases and found that during the minimum phase storms occur less often and in general have less severity. In particular, no storm with $D_{st,min} < -250$ nT was found during a minimum phase. On the con-

trary, during maximum phases we found the highest occurrence of severe storms. In the case of ascending phase, characterized by enhanced activity through flares and CMEs, the number of geomagnetic storms can be ordered by SC sunspots activity for moderate events but the statistics tend to be similar for more severe events. For descending phases, moderate and intense events are more likely to occur, and the storm rate occurrence is very similar to all SCs no matter how strong the SC was. One reason could be that in this phase the number of coronal holes is larger, in addition to they commonly migrates near equator spraying Earth with fast solar wind high speed streams. Their presence is related to sunspot presence, generating weak geomagnetic storms. However, we have found a possible correlation between the occurrence of storms during the descending phase of a cycle and the occurrence rate of events during the next solar maximum. This connection may be useful to make projections about the strength of the following cycle once the descending phase of the current cycle has finished.

Considering that geomagnetic storms can be modeled as stochastic processes with a log-normal probability distribution over their minimum D_{st} index, the data were separated according to SC and SC phases and fitted through ML method in order to characterize the occurrence of storms in each cycle and phase, and also make bootstrap extrapolations about the occurrence rate of severe and extreme events. We have computed the average waiting time between events, and have found that there is a good connection between the strength of the cycle in terms of sunspots and the occurrence of geomagnetic storms, even for moderate events. Namely, whereas for SC19, SC21, SC22, and SC23 the average waiting time between moderate storms is between 11 and 22 days, for the same kind of event the waiting time during SC20 and SC24 is between 18–26 and 18–29 days, respectively. Furthermore, these differences increases with increasing severity of the storm, such that the extrapolation of log-normal fits for SC20 and SC23 predicts the occurrence of extreme events with $D_{st,min} < -850$ nT every $(6.5 \pm 2.2) \times 10^4$ and $(1.6 \pm 0.5) \times 10^3$ years, respectively.

On the other hand, separating the events by SC phase, our results also show that maximum and minimum phases have the most and least occurrence of events regardless of the severity of the storms. Regarding ascending and descending phases, the results are similar for moderate storm but differ for stronger events, the occurrence rate during descending phase is always larger and the differences increases with decreasing $D_{st,min}$ (higher severity). In particular, our estimations predict events with $D_{st,min} < -300$ nT occurring every $3.6 \pm 0.7, 12.3 \pm 2.6, 42.3 \pm 11.6$, and 208 ± 63 years during maximum, descending, ascending, and minimum phases. Moreover, for extreme events our results predict the occurrence of geomagnetic storms reaching $D_{st,min} < -600$ nT approximately once every 126 ± 34 yr during maximum phase, but once every 926 ± 274, $(1.6 \pm 0.5) \times 10^4$, or $(6.8 \pm 2.2) \times 10^4$ yr, during descending, ascending, or minimum phases, respectively. Furthermore, comparing same phases of different SCs with each other we obtained that maximum and minimum phases tend to be ordered by the size of the SC measured by the number of sunspots, and that such order seems to be independent of the severity of the storms. For ascending phases the occurrence of moderate events also tend to be ordered by the sunspot number counts of each cycle, but this is not the case for stronger events. Finally, for descending phases differences are scarce and all cycles share similar results. However, the ordering of the cycles seem to exhibit a one-cycle delay between a given descending phase and the following maximum.

When we compared each SC with SC24 we can see that SC24 is very similar so SC20, in spite that the number of CMEs that occurred during SC24 was more similar to SC23. This can be explained by the relatively reduced field strength and speed of magnetic clouds that hit the Earth during this cycle (Gopalswamy et al., 2015). Therefore, when we try to establish a prediction of SC24 based on the activity during SC19–SC23, we tend to overestimate the actual numbers, as previous SCs were all more active than SC24. Actually, the occurrence of storms during SC24 turned out to be similar to the average occurrence rate during minimum phases of SCs. A possible explanation of this behavior may be related to the fact that, in general, the number of storms increase with increasing SSN, and the number of sunspot during SC24 was the lowest of all considered SCs. In relation of a prediction for SC25, we have found that bootstrap predictions of the strength of the next SC in terms of the expected occurrence of severe events, show that only the statistics of descending and maximum phases project large geomagnetic storms to occur at least once during the duration of a SC. Under this context, by looking at the σ value characteristic of the occurrence rate of storms, we have found that the σ_{des} shows the highest correlation with σ_{max} which allows us to attempt a prediction of

the maximum smoothed monthly sunspot number for SC25 to be between 150 and 200, therefore suggesting that the occurrence rate of storms for SC25 to be smaller than SC21, SC22, and SC23, but a more active than SC20 and SC24 that just ended. It is reasonable to be skeptical about the validity of such prediction based on such a low number of measurements, but our results also build on the connections found by other authors between descending phase and the following maximum phase (Dikpati et al., 2019; Feynman & Yue Gu, 1986; Leamon et al., 2020; McIntosh et al., 2019; McIntosh & Leamon, 2017). Naturally, as more data is collected (and of course as the true maximum of SC25 SSN is reached) it should be possible to test the scope and validity of this method.

Data Availability Statement

Sunspot data were obtained from the World Data Center SILSO, Royal Observatory of Belgium, Brussels. The D_{st} index used in this study was provided by the WDC for Geomagnetism, Kyoto (http://wdc.kugi.kyoto-u.ac.jp/wdc/Sec3.html). The complete list of geomagnetic storms; the list of solar cycles and solar cycle phases beginning dates, ending dates and duration; and the obtained parameters of each log-normal fit can be found in the Supporting Information S1.

Acknowledgments
The authors thank the World Data Center SILSO of the Royal Observatory of Belgium and the WDC for Geomagnetism at Kyoto for providing the data used in this study.

References

Baker, D. N., Daly, E., Daglis, I., Kappenman, J. G., & Panasyuk, M. (2004). Effects of space weather on technology infrastructure. *Space Weather*, *2*. https://doi.org/10.1029/2003SW000044

Bhowmik, P., & Nandy, D. (2018). Prediction of the strength and timing of sunspot cycle 25 reveal decadal-scale space environmental conditions. *Nature Communications*, *9*(1), 5209. https://doi.org/10.1038/s41467-018-07690-0

Borovsky, J. E., & Denton, M. H. (2016). Compressional perturbations of the dayside magnetosphere during high-speed-stream-driven geomagnetic storms. *Journal of Geophysical Research: Space Physics*, *121*, 4569–4589. https://doi.org/10.1002/2015JA022136

Cattell, C., Breneman, A., Colpitts, C., Dombeck, J., Thaller, S., Tian, S., et al. (2017). Dayside response of the magnetosphere to a small shock compression: Van Allen Probes, magnetospheric multiscale, and GOES-13. *Geophysical Research Letters*, *44*, 8712–8720. https://doi.org/10.1002/2017GL074895

Chapman, S. C., Horne, R. B., & Watkins, N. W. (2020). Using the index over the last 14 Solar cycles to characterize extreme geomagnetic activity. *Geophysical Research Letters*, *47*, e2019GL086524. https://doi.org/10.1029/2019GL086524

Dikpati, M., McIntosh, S. W., Chatterjee, S., Banerjee, D., Yellin-Bergovoy, R., & Srivastava, A. (2019). Triggering the birth of new cycle's sunspots by solar tsunami. *Scientific Reports*, *9*(1), 2035. https://doi.org/10.1038/s41598-018-37939-z

Eastwood, J. P., Biffis, E., Hapgood, M. A., Green, L., Bisi, M. M., Bentley, R. D., et al. (2017). The economic impact of space weather: Where do we stand? *Risk Analysis*, *37*, 206–218. https://doi.org/10.1111/risa.12765

Engebretson, M. J., Lessard, M. R., Bortnik, J., Green, J. C., Horne, R. B., Detrick, D. L., et al. (2008). Pc1-Pc2 waves and energetic particle precipitation during and after magnetic storms: Superposed epoch analysis and case studies. *Journal of Geophysical Research*, *113*, A01211. https://doi.org/10.1029/2007JA012362

Feynman, J., & Yue Gu, X. (1986). Prediction of geomagnetic activity on time scales of one to ten years. *Reviews of Geophysics*, *24*(3), 650–666. https://doi.org/10.1029/RG024i003p00650

Ganushkina, N., Jaynes, A., & Liemohn, M. (2017). Space weather effects produced by the ring cuurrent particles. *Space Science Reviews*, *212*, 1315–1344. https://doi.org/10.1007/s11214-017-0412-2

Gonzalez, W. D., Joselyn, J. A., Kamide, Y., Kroehl, H. W., Rostoker, G., Tsurutani, B. T., & Vasyliunas, V. M. (1994). What is a geomagnetic storm? *Journal of Geophysical Research*, *99*, 5771. https://doi.org/10.1029/93JA02867

Gopalswamy, N., Akiyama, S., Yashiro, S., Xie, H., Makela, P., & Michalek, G. (2015). *The mild space weather in solar cycle 24*.

Gosling, J. T., McComas, D. J., Phillips, J. L., & Bame, S. J. (1991). Geomagnetic activity associated with earth passage of interplanetary shock disturbances and coronal mass ejections. *Journal of Geophysical Research*, *96*, 7831. https://doi.org/10.1029/91JA00316

Hayakawa, H., Ebihara, Y., Willis, D. M., Hattori, K., Giunta, A. S., Wild, M. N., et al. (2018). The great space weather event during 1872 February recorded in East Asia. *Acta Pathologica Japonica*, *862*, 15. https://doi.org/10.3847/1538-4357/aaca40

Hynönen, R. (2013). *Geomagnetic activity and its sources during modern solar maximum (M.S. thesis)*. University of Helsinki.

Kamide, Y. & Chian, A. (2007). *Handbook of the solar-terrestrial environment*. Springer. https://doi.org/10.1007/978-3-540-46315-3

Kilpua, E. K. J., Olspert, N., Grigorievskiy, A., Käpylä, M. J., Tanskanen, E. I., Miyahara, H., et al. (2015). Statistical study of strong and extreme geomagnetic disturbances and solar cycle characteristics. *Acta Pathologica Japonica*, *806*, 272. https://doi.org/10.1088/0004-637X/806/2/272

Kreiss, J.-P., & Lahiri, S. N. (2012). 1—Bootstrap methods for time series. In *Handbook of Statistics* (Vol. 30, pp. 3–26). Elsevier. https://doi.org/10.1016/b978-0-444-53858-1.00001-6

Le, G.-M., Cai, Z.-Y., Wang, H.-N., Yin, Z.-Q., & Li, P. (2013). Solar cycle distribution of major geomagnetic storms. *Research in Astronomy and Astrophysics*, *13*, 739–748. https://doi.org/10.1088/1674-4527/13/6/013

Leamon, R. J., McIntosh, S. W., Chapman, S. C., & Watkins, N. W. (2020). Timing terminators: Forecasting sunspot cycle 25 onset. *Solar Physics*, *295*(2), 36. https://doi.org/10.1007/s11207-020-1595-3

Longden, N., Denton, M. H., & Honary, F. (2008). Particle precipitation during ICME-driven and CIR-driven geomagnetic storms. *Journal of Geophysical Research*, *113*, A06205. https://doi.org/10.1029/2007JA012752

Love, J. J., Rigler, E. J., Pulkkinen, A., & Riley, P. (2015). On the lognormality of historical magnetic storm intensity statistics: Implications for extreme-event probabilities. *Geophysical Research Letters*, *42*, 6544–6553. https://doi.org/10.1002/2015GL064842

McIntosh, S. W., Chapman, S., Leamon, R. J., Egeland, R., & Watkins, N. W. (2020). Overlapping magnetic activity cycles and the sunspot number: Forecasting sunspot cycle 25 amplitude. *Solar Physics*, *295*(12), 163. https://doi.org/10.1007/s11207-020-01723-y

McIntosh, S. W., & Leamon, R. J. (2017). Deciphering solar magnetic activity: Spotting solar cycle 25. *Frontiers in Astronomy and Space Sciences*, *4*, 4. https://doi.org/10.3389/fspas.2017.00004

McIntosh, S. W., Leamon, R. J., Egeland, R., Dikpati, M., Fan, Y., & Rempel, M. (2019). What the sudden death of solar cycles can tell us about the nature of the solar interior. *Solar Physics*, *294*(7), 88. https://doi.org/10.1007/s11207-019-1474-y

Moya, P. S., Pinto, V. A., Sibeck, D. G., Kanekal, S. G., & Baker, D. N. (2017). On the effect of geomagnetic storms on relativistic electrons in the outer radiation belt: Van Allen probes observations. *Journal of Geophysical Research: Space Physics*, *122*, 11100–11108. https://doi.org/10.1002/2017JA024735

Pulkkinen, A., Lindahl, S., Viljanen, A., & Pirjola, R. (2005). Geomagnetic storm of 29–31 October 2003: Geomagnetically induced currents and their relation to problems in the Swedish high-voltage power transmission system. *Space Weather*, *3*, S08C03. https://doi.org/10.1029/2004SW000123

Pulkkinen, A., Pirjola, R., & Viljanen, A. (2008). Statistics of extreme geomagnetically induced current events. *Space Weather*, *6*, S07001. https://doi.org/10.1029/2008SW000388

Reyes, P., Pinto, V. A., & Moya, P. S. (2019). Statistical analysis of geomagnetic storms and their relation with the solar cycle. *Proceedings of the International Astronomical Union*, *15*(S354), 224–227. https://doi.org/10.1017/S1743921320000903

Riley, P., & Love, J. J. (2017). Extreme geomagnetic storms: Probabilistic forecasts and their uncertainties. *Space Weather*, *15*, 53–64. https://doi.org/10.1002/2016SW001470

Shepherd, S. J., Zharkov, S. I., & Zharkova, V. V. (2014). Prediction of solar activity from solar background magnetic field variations in cycles 21–23. *The Astrophysical Journal*, *795*(1), 46. https://doi.org/10.1088/0004-637x/795/1/46

Shi, Y., Zesta, E., & Lyons, L. R. (2008). Modeling magnetospheric current response to solar wind dynamic pressure enhancements during magnetic storms: 1. Methodology and results of the 25 September 1998 peak main phase case. *Journal of Geophysical Research*, *113*, A10218. https://doi.org/10.1029/2008JA013111

SILSO World Data Center. (1957–2019). *The international sunspot number. International sunspot number monthly bulletin and online catalogue*. SILSO World Data Center.

Siscoe, G., Crooker, N., & Clauer, C. (2006). Dst of the carrington storm of 1859. *Advances in Space Research*, *38*(2), 173–179. https://doi.org/10.1016/j.asr.2005.02.102

Stepanova, M., Antonova, E., Moya, P., Pinto, V., & Valdivia, J. (2019). Multisatellite analysis of plasma pressure in the inner magnetosphere during the 1 June 2013 geomagnetic storm. *Journal of Geophysical Research: Space Physics*, *124*, 1187–1202. https://doi.org/10.1029/2018JA025965

Svalgaard, L., Cliver, E. W., & Kamide, Y. (2005). Sunspot cycle 24: Smallest cycle in 100 years? *Geophysical Research Letters*, *32*(1), L01104. https://doi.org/10.1029/2004GL021664

Tandberg-Hanssen, E., & Emslie, A. G. (1988). *The physics of solar flares*. Cambridge University Press.

Turner, D. L., Kilpua, E. K. J., Hietala, H., Claudepierre, S. G., O'Brien, T. P., Fennell, J. F., et al. (2019). The response of Earth's electron radiation belts to geomagnetic storms: Statistics from the Van Allen probes era including effects from different storm drivers. *Journal of Geophysical Research: Space Physics*, *124*, 1013–1034. https://doi.org/10.1029/2018JA026066

Turner, D. L., O'Brien, T. P., Fennell, J. F., Claudepierre, S. G., Blake, J. B., Kilpua, E. K. J., & Hietala, H. (2015). The effects of geomagnetic storms on electrons in Earth's radiation belts. *Geophysical Research Letters*, *42*, 9176–9184. https://doi.org/10.1002/2015GL064747

World Data Center for Geomagnetism, Kyoto. Nose, M., Iyemori, T., Sugiura, M., & Kamei, T. (2015). *Geomagnetic Dst index*. https://doi.org/10.17593/14515-74000

Wrenn, G. L. (2009). Chronology of "killer" electrons: Solar cycles 22 and 23. *Journal of Atmospheric and Solar-Terrestrial Physics*, *71*, 1210–1218. https://doi.org/10.1016/j.jastp.2008.08.002

Wrenn, G. L., Rodgers, D. J., & Ryden, K. A. (2002). A solar cycle of spacecraft anomalies due to internal charging. *Annales Geophysicae*, *20*, 953–956. https://doi.org/10.5194/angeo-20-953-2002

Zhuang, B., Wang, Y., Shen, C., Liu, R., & Liu, R. (2018). A statistical study of the likelihood of a super geomagnetic storm occurring in a mild solar cycle. *Earth and Planetary Physics*, *2*, 112–119. https://doi.org/10.26464/epp2018012